THE JOURNAL OF PHYSICAL CHEMISTRY B

Article

pubs.acs.org/JPCB

Accurate Determination of the Orientational Distribution of a Fluorescent Molecule in a Phospholipid Membrane

Štěpán Timr,[†] Alexey Bondar,[‡,§] Lukasz Cwiklik,[†,∥] Martin Štefl,[∥] Martin Hof,[∥] Mario Vazdar,[⊥] Josef Lazar,*[,‡,§] and Pavel Jungwirth*[,†,#]

[†]Institute of Organic Chemistry and Biochemistry, Academy of Sciences of the Czech Republic, Flemingovo nám. 2, 16610 Prague 6, Czech Republic

[‡]Institute of Nanobiology and Structural Biology GCRC, Academy of Sciences of the Czech Republic, v.v.i., Zámek 136, 37333 Nové Hrady, Czech Republic

[§]Faculty of Science, University of South Bohemia, Branišovská 31, 37005 České Budějovice, Czech Republic

[∥]J. Heyrovský Institute of Physical Chemistry, Academy of Sciences of the Czech Republic, v.v.i., Dolejškova 3, 182 23 Prague 8, Czech Republic

[⊥]Rudjer Bošković Institute, Division of Organic Chemistry and Biochemistry, POB 180, HR-10002 Zagreb, Croatia

[#]Department of Physics, Tampere University of Technology, P.O. Box 692, FI-33101 Tampere, Finland

Supporting Information

ABSTRACT: Orientation of lipophilic dye molecules within a biological membrane can report on the molecular environment, i.e., the physical and chemical properties of the surrounding membrane. This fact, however, remains under-utilized, largely because of our limited quantitative knowledge of molecular orientational distributions and the fact that robust techniques allowing experimental observation of molecular orientations of dyes in biological membranes are only being developed. In order to begin filling this lack of knowledge and to develop appropriate tools, we have investigated the membrane orientational distribution of the 3-hydroxyflavone-based membrane dye F2N12S. Results of our single- and two-photon polarization microscopy observations of linear dichroism of F2N12S-labeled giant unilamellar vesicles are consistent with a Gaussian-like orientational distribution of the transition dipole moment of the dye, with a mean tilt angle of 53.2 ± 0.1° with respect to the bilayer normal and a standard deviation of 13.3 ± 0.6°. Independently, by combining quantum chemical calculations and molecular dynamics simulations, we obtained very similar values; a mean tilt angle of 48 ± 4° and a standard deviation of 13 ± 2°. The good agreement between the experimentally and computationally obtained values cross-validates both approaches and gives confidence to the results obtained. The results open a door to robust quantitative determinations of orientational distributions of fluorescent molecules (ranging from simple synthetic dyes to fluorescent proteins attached to membrane proteins) associated with lipid membranes. Such determinations enable rational development of a novel class of sensitive fluorescent optical probes, reporting on cellular events through changes in linear dichroism.

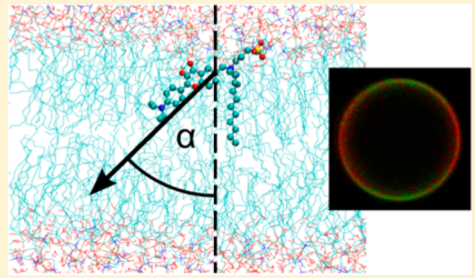

INTRODUCTION

The past several decades have witnessed a tremendous interest in development of new, improved fluorescent sensors of biological and biophysical processes, both synthetic and genetically encoded.[1] The fluorescence property used for detection depends on the particular feature or process being observed, and on the particular fluorescent sensor being used. Properties commonly exploited in fluorescent sensors include: (i) overall fluorescence emission intensity, (ii) excitation or emission spectra, (iii) fluorescence lifetime, or (iv) fluorescence anisotropy (FA).[2−4] While variations in the former three observables are largely due to changes in the electronic structure of the fluorophore, FA reports on molecular orientation and molecular rotation.[5,6]

Recent work by us[7] and others[8−10] has involved yet another mode of fluorescence reporting − fluorescence detected linear dichroism (FDLD). In LD measurements, differences in absorption of light of mutually perpendicular (or multiple) polarizations are being conveniently measured through observations of the corresponding fluorescence intensities. Unlike FA, FDLD is not suitable for investigating molecular processes involving molecules in solution. However, in observations of fluorescently labeled membranes, filaments, or other microscopic structures, FDLD presents several important advantages over FA that make FDLD measurements substantially more sensitive and, therefore, open up a large number of new applications.[7,11] Namely, FDLD is unaffected by noncollinearity of excitation and emission transition dipole

Received: July 8, 2013
Revised: November 20, 2013
Published: November 21, 2013

moments (TDM), and neither is it affected by molecular rotation between the events of excitation and emission. In fact, not being dependent on the angular rotational rate, FDLD reports purely on molecular orientation and, therefore, offers unambiguous interpretation of measurements. Furthermore, FDLD observations can be made using high numerical aperture objective lenses, which are needed for efficient collection of fluorescence from biological samples, which is also aided by absence of polarization optical components in the emission pathway. Although FDLD measurements are affected by dispersion of the excitation light, they are largely unaffected by dispersion of fluorescence by the sample.

While microscopic FDLD imaging is more difficult to implement than FA imaging due to a need to modulate the excitation light polarization, the difficulty has been overcome by beam multiplexing[10] and electro-optical polarization modulation.[7] Microscopic FDLD measurements often take advantage of optical sectioning abilities, such as those of total internal reflection fluorescence (TIRF) microscopy or of point scanning fluorescence microscopy techniques (single-photon (1P) confocal, two-photon (2P)). Using electro-optical polarization modulation allows facile and sensitive microscopic observations of FDLD in living cells and animals, even labeled at low levels with genetically encoded fluorescent proteins. Changes in FDLD in fluorescently labeled proteins have now been used to report, with high sensitivity, on molecular processes these proteins undergo.[7,9,12] Through changes in protein conformation, several processes of high scientific interest such as variations in intracellular calcium concentration, activation of G-protein signaling, or changes in cell membrane voltage[12] have been visualized. Due to its favorable properties and the importance of its biological imaging applications, FDLD microscopy is likely to become a major imaging tool, used for sensitive detection of various membrane biophysical properties that affect molecular orientation, both of fluorescent proteins and of fluorescent dyes.

Apart from allowing qualitative observations of changes in molecular orientation, FDLD measurements should also allow for quantitative determinations of molecular orientations of fluorescent molecules within lipid membranes in giant unilamellar vesicles (GUVs) and, ultimately, in living cells and organisms. This capability may become valuable in rational development of fluorescent probes, particularly genetically encoded ones. Considerable progress in this area has already been made. One-photon confocal and two-photon FDLD measurements, in combination with second harmonic generation, have been used to infer parameters of an orientational distribution (i.e., the mean tilt angle with respect to the bilayer normal and its standard deviation) of the one-photon excitation transition dipole moment (1PE TDM) of a dye (di-4-ANEPPS) incorporated in GUVs.[11] Similarly, 2P polarimetric analysis has been used to derive parameters of orientational distribution of the synthetic dyes Laurdan, C-Laurdan, di-8-ANEPPQ, and TA-DPH, in vesicles and cells.[13] Polarized TIRF microscopy measurements of molecular assemblies and single fluorescent molecules embedded in lipid membranes have allowed one to obtain parameters of orientational distributions of dyes such as DiI or BODIPY. What is, however, missing is a quantitative verification of the orientational distribution parameters by independent means, needed to show that assumptions made in structural interpretations of FDLD microscopy data are justified. These assumptions include smoothness of the GUV membrane, vector-like behavior of the 2P absorptivity tensor, Gaussian distribution of the fluorophore orientations, and absence of interference with the membrane structure by the intense illumination used for 2P excitation.

One such verification has been attempted for the dye DiI-C18(3), through molecular dynamics simulations of the dye embedded in a phosphatidyl choline membrane.[14] However, the convergence of the simulations was limited, the corresponding pioneering measurements were made[15] for different systems with chemically complex membranes of biological origin, and at a time that allowed only limited interpretation in terms of molecular orientation distribution. Therefore, the validity of determinations of orientational distributions of fluorescent molecules within lipidic membranes through optical microscopy remains to be independently verified.

In order to close this gap in knowledge and to establish the ability of FDLD microscopy to yield accurate information on orientational distributions of fluorescent molecules in membranes, we characterize here such a distribution of a fluorescent dye in a model membrane system through FDLD measurements and, independently, via a combination of quantum mechanical (QM) calculations and molecular dynamics (MD) simulations. Our model membrane system consists of GUVs composed of 1-palmitoyl-2-oleoylphosphatidylcholine (POPC), and the selected fluorescent molecule is a 3-hydroxyflavone dye, namely, *N*-[[4′-*N*,*N*-diethylamino-3-hydroxy-6-flavonyl]-methyl]-*N*-methyl-*N*-(3-sulfopropyl)-1-dodecanaminium (F2N12S); see Figure 1. F2N12S is a member of a recently developed family of bright (both with 1P and 2P excitations) membrane staining dyes, sensing polarity and hydration of lipid membranes via a mechanism involving an excited state intramolecular proton transfer and formation of hydrogen bonds with water, potentially accompanied by changes in molecular orientation.[16−19] F2N12S has been used in detection of apoptotic cell death,[20] to visualize lipid domains in GUVs,[21]

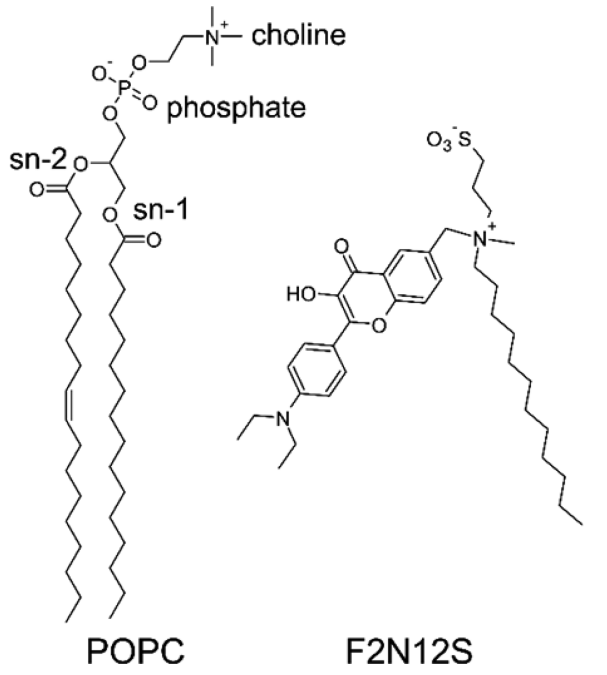

Figure 1. Molecular structures of the membrane-forming phospholipid POPC and the fluorescent dye F2N12S.

dx.doi.org/10.1021/jp4067026 | J. Phys. Chem. B 2014, 118, 855−863

and to provide evidence for lipid domains in the outer leaflet of cell membranes.[22] For the purpose of the present study it is important that the molecular structure of F2N12S is also suitable for QM calculations, and for MD simulations of the dye embedded in a lipid bilayer. Furthermore, its excitation spectrum, exhibiting a single absorption transition, allows simple interpretation of FDLD measurements in terms of a single excitation TDM.

METHODS

Interpretation of FDLD Data in Terms of Molecular Orientation. The absorption probability of a linearly polarized light by a molecule in a process of 1P excitation (1PE) is proportional to $\cos^2 \beta$, where β is an angle between the 1PE TDM of the molecule and the direction of the electric field vector. The observed intensity of fluorescence is then[10,23,24]

$$I^{(1P)} = I_0 \cos^2 \beta \tag{1}$$

where I_0 is the intensity of the emitted light when the fluorophore transition moment and the polarization of the incident light are aligned.

Although 2P absorption properties are generally determined by a transition tensor rather than a vector, for certain molecules, including F2N12S, a vector description using the 1PE TDM is applicable as an approximation.[25−27] These molecules are characterized by a significant difference between the electric dipole moments of the ground and excited state which is, moreover, parallel to the corresponding 1PE TDM.[25−27] In these cases, the transition tensor has a dominant contribution proportional to the 1PE TDM. In contrast to 1P excitation, the 2P absorption probability depends on the fourth power of cos β[10,24]

$$I^{(2P)} = I_0 \cos^4 \beta \tag{2}$$

In our experiments, FDLD was quantified using the dichroic ratio r, defined as

$$r = I_h/I_v \tag{3}$$

where I_h and I_v are intensities of fluorescence excited with light polarized in two orthogonal directions (horizontal and vertical in the images), lying in the focal plane of the objective. We described the orientation of the 1PE TDM of dye molecules embedded in the membrane with a tilt angle α (between 0° and 90°) with respect to the membrane normal, integrating over angle ρ corresponding to the rotation around the normal.[15] The direction of the membrane normal relative to a Cartesian coordinate system (with the x and y axes being parallel to the horizontal and vertical polarizations, respectively, and the z axis aligned with the laser beam) was expressed by angles θ and φ as depicted in Figure 2. Since we imaged GUVs in their equatorial planes, we treated φ as being equal to zero. Consequently, the following formulas for the intensities of fluorescence resulting from a 1P excitation with light polarized in the horizontal and vertical direction were used:[11]

$$I_h^{(1P)}(\theta) = I_0(\langle\cos^2 \alpha\rangle\cos^2 \theta + 1/2\langle\sin^2 \alpha\rangle\sin^2 \theta) \tag{4a}$$

$$I_v^{(1P)}(\theta) = I_0(\langle\cos^2 \alpha\rangle\sin^2 \theta + 1/2\langle\sin^2 \alpha\rangle\cos^2 \theta) \tag{4b}$$

Here, angle brackets represent expectation values determined by the characteristic distribution of the tilt angle α. For 2P excitation, the following relations apply:[11]

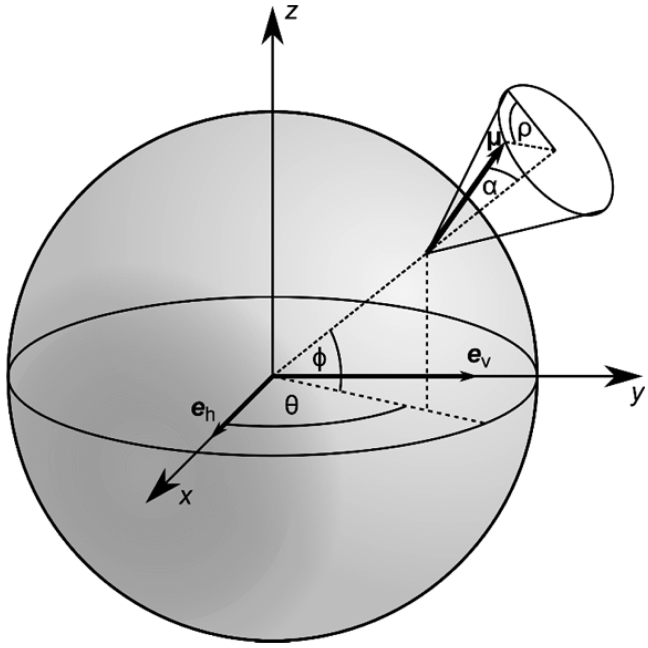

Figure 2. Geometrical model of the 1PE TDM orientation of a fluorescent probe embedded in a membrane, similar to that in refs 13,15. Vectors $\mathbf{e}_h$ and $\mathbf{e}_v$ show directions of the horizontal and vertical polarization.

$$I_h^{(2P)}(\theta) = I_0(\langle\cos^4 \alpha\rangle\cos^4 \theta + 3/16\langle\sin^2 2\alpha\rangle\sin^2 2\theta + 3/8\langle\sin^4 \alpha\rangle\sin^4 \theta) \tag{5a}$$

$$I_v^{(2P)}(\theta) = I_0(\langle\cos^4 \alpha\rangle\sin^4 \theta + 3/16\langle\sin^2 2\alpha\rangle\sin^2 2\theta + 3/8\langle\sin^4 \alpha\rangle\cos^4 \theta) \tag{5b}$$

The dichroic ratio r (eq 3) was measured along GUV membranes as a function of angle θ. Theoretical predictions of $\log_2 r$ (θ) for 1P and 2P excitation, derived using eqs 4a,4b and 5a,5b, respectively, were fitted to experimental data. Two expectation values of $\cos^2 \alpha$ and $\cos^4 \alpha$ (the remaining expectation values being dependent on them) were obtained from a combination of 1P and 2P measurements as independent parameters characterizing the distribution of α. The distribution of α was assumed in the form

$$F(\alpha) = f(\alpha)\sin \alpha \tag{6}$$

where the sin α term reflects the change in density of states with α.

On the basis of experimental data, $f(\alpha)$ was approximated in three different ways, using a Gaussian function, an entropy maximizing function, and a truncated Legendre polynomial expansion. In the Gaussian approximation, $F(\alpha)$ was described as

$$F(\alpha) \approx F_G(\alpha) = A \exp\left(-\frac{(\alpha - \alpha_0)^2}{2\sigma^2}\right)\sin \alpha \tag{7}$$

Here, A is a normalization factor, and parameters α_0 and σ determine the position and width of the Gaussian distribution. Note that due to the presence of the sin α term in eq 7, α_0 and σ no longer directly correspond to the mean and standard deviation of the tilt angle distribution.

Within another approach requiring $f(\alpha)$ to maximize entropy, we used an orientational distribution in the following form:

dx.doi.org/10.1021/jp4067026 | J. Phys. Chem. B 2014, 118, 855−863

$$F_S(\alpha) = Be^{(\lambda_2 P_2(\cos\alpha)+\lambda_4 P_4(\cos\alpha))}\sin\alpha \quad (8)$$

where B is a normalization factor, $P_2(\cos\alpha)$ and $P_4(\cos\alpha)$ are Legendre polynomials in cos α of the second and fourth order, respectively,

$$P_2(\cos\alpha) = \frac{1}{2}(3\cos^2\alpha - 1) \quad (9)$$

$$P_4(\cos\alpha) = \frac{1}{8}(35\cos^4\alpha - 30\cos^2\alpha + 3) \quad (10)$$

and parameters λ_2 and λ_4 are determined on the basis of the constraints obtained from experiments.[28,29]

As the third possibility, we approximated $f(\alpha)$ with a truncated Legendre polynomial expansion. Thus,

$$F(\alpha) \approx F_L(\alpha) = [1 + 5\langle P_2\rangle P_2(\cos\alpha) + 9\langle P_4\rangle P_4(\cos\alpha)]\sin\alpha \quad (11)$$

where $\langle P_2\rangle$ and $\langle P_4\rangle$ are the expectation values of $P_2(\cos\alpha)$ and $P_4(\cos\alpha)$, which can be expressed in terms of $\langle\cos^2\alpha\rangle$ and $\langle\cos^4\alpha\rangle$.

MD Simulations. Classical MD simulations were performed using the program GROMACS 4.5.2.[30] A periodic box containing a single F2N12S molecule, 128 POPC molecules forming a bilayer, and 8952 water molecules was simulated. Four different sets of initial conditions were prepared with the dye molecule inserted into the vicinity of the membrane, with its alkyl chain being either inside or outside the bilayer. After energy minimization and a short 10 ns equilibration period, 500 ns runs were performed at constant pressure and temperature for each set of initial conditions. A time step of 2 fs was employed. Temperature of 310 K (i.e., increased by 17 °C in comparison to experiments to speed up sampling) was maintained by the Nosé-Hoover thermostat[31] with a time constant τ_T = 1 ps, while pressure was kept at 1.01 bar by the Parrinello-Rahman barostat[32] with a time constant τ_p = 2 ps. The LINCS algorithm[33] was employed for constraining the bond lengths of F2N12S and POPC molecules, while the bond lengths of water molecules were constrained with the SETTLE algorithm.[34] The nonbonded interaction cutoff was set to 1 nm, and the long-range electrostatic interactions were accounted for using the particle mesh Ewald method[35] with grid spacing of 0.12 nm and fourth-order interpolation.

In order to construct force field parameters for the F2N12S dye, we first performed ab initio geometry optimization of the dye molecule with a shorter four-carbon alkyl chain in place of the original twelve-carbon chain. The B3LYP functional[36] with the cc-pVDZ basis set[37] was employed within the Gaussian 09 program.[38] Atomic charges were subsequently obtained from the Merz−Kollman−Singh ESP fit[39] for the optimized structure. After removing the terminal CH_3 group of the shortened alkyl chain of the optimized structure and adding the missing nine CH_n groups, the PRODRG2 server[40] was employed to generate a GROMACS topology file based on the united-atom GROMOS-87 force field[41] with corrections detailed in refs 42,43. To ensure consistency in interactions with membrane phospholipids, the default CH2 and CH3 united-atom types of the alkyl chain were replaced with the LP2 and LP3 atom types adopted from the united-atom Berger lipids force field.[44] The nine terminal CH_n groups of the alkyl chain were given a zero charge, in accord with the Berger lipids force field, and the charges of the second and the third CH_2 groups were decreased by 0.03e to ensure neutrality of the whole structure. Furthermore, the dihedral potentials assigned to five dihedral angles of the molecule were modified on the basis of quantum calculations (for details see Supporting Information). POPC molecules were described using the Berger lipids force-field[44] and water using the SPC model.[45]

1PE TDM Calculations. To determine the mean orientation of the 1PE TDM relative to the molecular geometry of the dye embedded in the bilayer, the 1PE TDM corresponding to the $S_0 \rightarrow S_1$ ($\pi \rightarrow \pi^*$) transition was calculated for a series of 87 randomly chosen snapshots from the four MD trajectories described above. The TD-DFT/B3LYP method[46−49] with the def2-SVP basis set[50] was employed with the nine terminal CH_n groups of the twelve-carbon alkyl chain being removed from the quantum system. The surrounding environment was modeled as point charges, an approach already used for calculating absorption and emission spectra of another polar probe (PRODAN) embedded in a phospholipid bilayer.[51] Hydrogen atoms were added to the united atom geometry of the dye using the Open Babel package.[52] The resulting direction of the 1PE TDM relative to the geometry of the molecule was described in terms of two angles, one between the projection of the 1PE TDM onto the plane of a selected aromatic ring and a vector connecting a pair of atoms of this aromatic ring, the other indicating the deviation of the 1PE TDM from the plane of the aromatic ring.

GUV Preparation. GUVs were prepared using the electroformation method[53] modified by Stöckl et al.[54] A mixture containing 97 mol % of POPC, 2 mol % of biotinylated DPPE, and 1 mol % of the F2N12S dye was prepared in a small glass test tube. The total lipid concentration was 200 nmol in 100 μL of chloroform. The lipid mixture was uniformly spread on two preheated (48 °C) titanium plate electrodes, 25 μL on each (for details of the chamber design see ref 54). The electrodes were placed in a desiccator and kept under vacuum for two hours. Next, the pair of electrodes was isolated using Parafilm, the swelling chamber was filled with 0.1 M of sucrose solution (Π = 103 mOsm), and a sinusoidal voltage was applied. The voltage and frequency sequences were as follows: (1) initiation stage with duration of 50 min, frequency of 10 Hz, and voltage being linearly raised in 50 mV intervals from 150 mV to 1.1 V; (2) GUVs formation stage with duration of 90 min, frequency of 10 Hz, and voltage of 1.1 V; (3) GUVs detaching with duration of 30 min, frequency of 4 Hz, and voltage of 1.3 V. The titanium electrodes were kept at 48 °C during the whole electroformation process. Newly formed GUVs were carefully transferred to an Eppendorf test tube, stored at room temperature, and used within three days. Prior to measurements, GUVs were diluted 20-fold in a glucose solution (60 mM glucose, 10 mM NaCl, 10 mM HEPES, Π = 103 mOsm) and pipetted (400 μL) into an imaging chamber (μ-Slide 8 well, iBidi, Germany) precoated with streptavidin bound to biotinylated albumin.

Microscopy and Image Processing. Polarization microscopy experiments were carried out on a custom-built confocal laser scanning microscope based on the iMic2 microscope (Till Photonics, Germany) at a temperature of 20 °C. Imaging was performed using a UApoPlan/IR × 60 NA1.2 water-immersion objective lens (Olympus, Japan). Polarization of the excitation beam was altered between horizontal and vertical directions by a polarization modulator (RPM-2P, Innovative Bioimaging, USA) operated at 100 kHz, synchronized with acquisition of

individual pixels by the microscope. The 1P setup is shown in Figure S3 in SI. Fluorescence was excited by a 405 nm laser (50 mW, PowerLaser, Czech Republic), with the beam diameter restricted by a pinhole to ~0.5 mm, so that the light emerging from the objective formed a narrow (~20°) cone. A 500 nm short-pass dichroic mirror placed outside the scanner was used to separate fluorescence from excitation light. Fluorescence was directed through a confocal pinhole (LSM410, Carl Zeiss, Germany) to a photomultiplier (R6357, Hamamatsu Photonics, Japan) equipped with a Brightline 542/27 emission filter (Semrock, USA). The 2P setup is shown in Figure S4 in Supporting Information. The Chameleon Ultra II laser (Coherent, Inc., USA) with GVD compensation was operated at 810 nm, and a 735 nm long-pass dichroic mirror (Semrock, USA) was used to separate fluorescence from excitation light. The photomultiplier was equipped with a short-pass HQ700SP-2P emission filter (Chroma, USA). Image deconvolution, processing, and analysis were performed in a manner similar to that described for 2P polarization microscopy.[7] Background was calculated as the mean pixel value of regions not containing any GUVs, and subtracted. A 3% correction for depolarization of the 405 nm laser beam by the optical setup was applied to the 1P data. A correction factor compensating for unequal intensities of the two perpendicular polarizations of the excitation beam was established from the fluorescence signal of an isotropic sample. GUV membranes were marked with splines obtained using the Active Cells plugin[55,56] of the image analysis software Icy.[57] For each polarization, the intensities of pixels located within a distance of five pixels from the spline were binned according to the angle of the spline normal relative to the horizontal direction. For each of these 3° bins, the value of the dichroic ratio was calculated. In order to account for polarization sensitivity of the emission pathway, we applied a correction that made the dichroic log ratio profiles be centered at zero. We quantitatively analyzed at least ten representative GUVs, both for 1P and 2P imaging experiments.

RESULTS AND DISCUSSION

Membrane Distribution of F2N12S from MD Simulations. To determine the molecular orientation of the F2N12S dye within the model membrane computationally, we employed a series of MD simulations. Four distinct sets of starting conditions with the dye initially in the aqueous phase all showed stabilization of the dye within the membrane no later than 150 ns after the beginning of the simulations. In two cases, the relocation proceeded through an intermediate state characterized by the aromatic rings being located in the polar part of the bilayer, the twelve-carbon alkyl chain embedded in the hydrophobic core of the membrane, and the diethylamine group pointing out of the membrane into the water environment. Ultimately, the aromatic rings adopted a tilted orientation with the diethylamine group directed toward the center of the bilayer, the SO_3^- group embedded in the polar part of the membrane, and the twelve-carbon alkyl chain located among acyl chains of the POPC molecules (Figure 3).

The last 300 ns of each of the 500 ns simulations, after the system equilibrated, were used for further analysis. The results of this analysis, in the form of density profiles of selected atoms or groups of the dye and lipid molecules, are summarized in Figure 4. The density profile of the ammonium nitrogen of the dye peaks at 1.30 nm from the bilayer center, i.e., below the average location of sn-1 and sn-2 carbonyl oxygen atoms of POPC. The density profile of the OH group of the dye acquires its maximum 1.25 nm from bilayer center, while the diethylamine nitrogen peaks much deeper at 0.65 nm. The SO_3^- group of the dye has a density profile with a maximum at 1.60 nm, i.e., at the same distance from the bilayer center as the sn-2 carbonyl oxygen and below the peaks of the phosphate phosphorus and choline nitrogen. However, a more detailed inspection reveals that the choline head groups of the neighboring POPC molecules can tilt down to interact with the SO_3^- group. Finally, the terminal C12 atom of the twelve-carbon alkyl chain exhibits a broad density profile with a peak at 0.25 nm, close to the center of the bilayer. Overall, we found the typical location of the dye to be deeper than anticipated in a previous experimental study,[20] which placed the ammonium nitrogen only slightly below the phosphate group and the other nitrogen somewhat below the sn-1 carbonyl oxygen. Additional results of the trajectory analysis, including detailed information on interactions of the dye within the bilayer, can be found in Supporting Information.

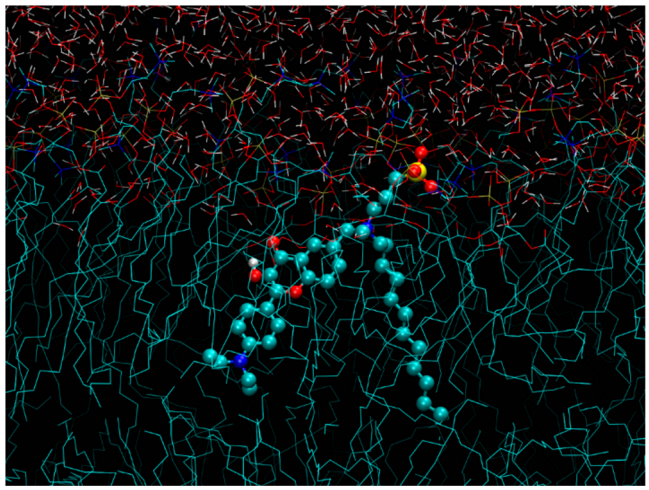

Figure 3. Cropped snapshot from a MD simulation showing a typical orientation of the F2N12S dye in POPC bilayer. Color coding: cyan, carbon; red, oxygen; white, hydrogen; blue, nitrogen; yellow, sulfur; and tan, phosphorus.

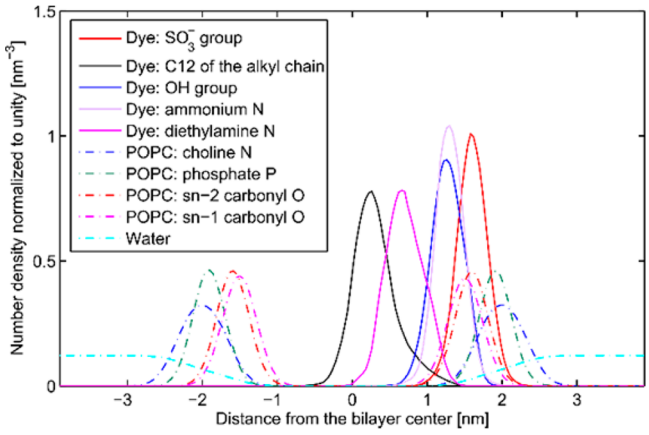

Figure 4. Total density profiles of selected atoms and groups of the system as a function of the distance from the bilayer center. The signal from the dye is only on one side of the bilayer since the dye never flipped across the membrane during the duration of the MD simulations. Note that the flip-flop kinetics of F2N12S was characterized experimentally previously.[58]

dx.doi.org/10.1021/jp4067026 | J. Phys. Chem. B 2014, 118, 855−863

Orientation of the 1PE TDM within the F2N12S Molecule. To determine the orientation of the 1PE TDM within the F2N12S molecule, we performed quantum chemistry calculations. The 1PE TDM vector was calculated for a set of geometries of the F2N12S dye randomly selected from the four performed MD simulations after localization of the dye inside the bilayer. Despite the differences in geometry and effects of the environment, the orientation of 1PE TDM with respect to the aromatic rings of the dye proved to be constant within a few degrees. Namely, the 1PE TDM orientation was described with in-plane and out-of-plane angles γ and δ (see Figure 5), with mean values of $\gamma = 9°$ and $\delta = 1°$,

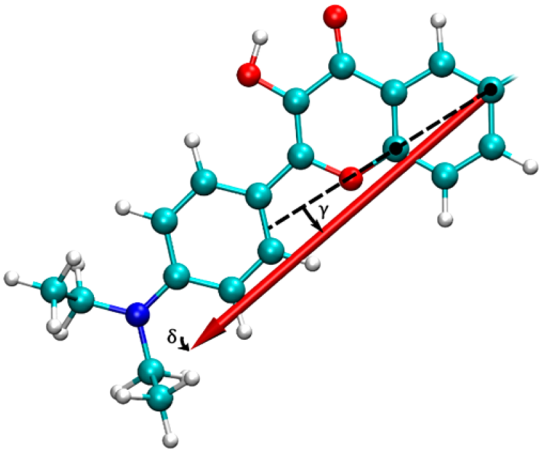

Figure 5. Mean 1PE TDM orientation within the frame of the aromatic rings of the F2N12S molecule. $\gamma = 9°$ is the angle between an axis defined by the two marked carbon atoms and the projection of the 1PE TDM onto the plane of the aromatic ring containing these two atoms; $\delta = 1°$ quantifies the deviation of the 1PE TDM from the plane of the aromatic ring.

and standard deviations $\sigma_\gamma = 2°$ and $\sigma_\delta = 5°$, respectively. Therefore, when computing the distribution of the 1PE TDM tilt angle α with respect to the membrane normal from MD simulations, we could safely assume that the orientation of the 1PE TDM relative to the aromatic rings was fixed at the mean values of γ and δ.

Orientational 1PE TDM Distribution from FDLD Measurements. In order to test the ability of FDLD measurements to yield accurate information on molecular orientation, we carried out 1P and 2P FDLD measurements on F2N12S stained GUVs, and used the resulting data to infer information on the orientational distribution of the F2N12S 1PE TDM within the lipid bilayer. In both measurements, we detected weak but clearly observable FDLD, with a maximum of $\log_2 r$ close to 0.25 (i.e., $r = 1.19$) for 1P excitation and 0.15 (i.e., $r = 1.11$) for 2P excitation. Examples of our imaging results are shown in Figure 6. By fitting 1P and 2P experimental data with functions based on the theoretical model described in Methods, we found $\cos^2 \alpha$ to be 0.374 ± 0.001 and $\cos^4 \alpha$ within 0.181 ± 0.002 (mean $\pm$ 2 $\times$ SEM), or, in terms of the expectation values of $P_2(\cos \alpha)$ and $P_4(\cos \alpha)$, $\langle P_2 \rangle = 0.061 \pm 0.002$ and $\langle P_4 \rangle = -0.234 \pm 0.010$.

Using the experimental values of $\langle \cos^2 \alpha \rangle$ and $\langle \cos^4 \alpha \rangle$, or equivalently, $\langle P_2 \rangle$ and $\langle P_4 \rangle$, we reconstructed the distribution of the tilt angle α in three different ways by fitting the experimental data with eqs 7, 8, or 11 (Figure 7A–C). In all three cases, the results show similarly shaped broad

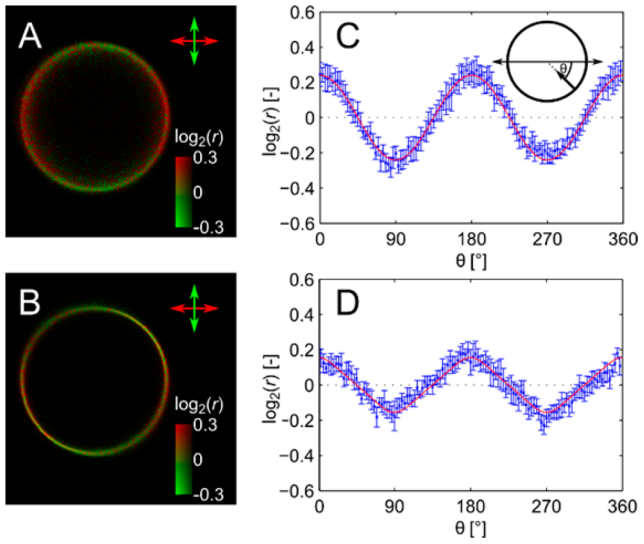

Figure 6. FDLD of F2N12S in POPC GUVs observed with 1P and 2P excitations. (A,B) Images of representative GUVs acquired using 1P and 2P excitation, respectively. Fluorescence intensity is indicated by brightness, dichroic ratio (in the form of $\log_2(r)$) by hue, as indicated by the color bars. The arrows show the directions of excitation beam polarization. (C,D) Plots showing the dependence of $\log_2(r)$ on the orientation of the membrane normal, as obtained from the series of 1P and 2P measurements, respectively. The red curves represent the theoretical model described in Methods fitted to the experimental data.

distributions of tilt angles with a single peak in the middle region of α. For the Gaussian approximation (Figure 7A), our FDLD measurements are consistent with α_0 within the 95% confidence interval of (50.2, 50.5)° and σ within (187.3 − 3.44 α_0, 187.9 − 3.44 α_0)°, yielding a mean tilt angle value of 53.2 $\pm$ 0.1° and a standard deviation of 13.3 $\pm$ 0.6°. The mean value and standard deviation of the distribution constructed by entropy maximization (Figure 7B), with $\lambda_2 = 0.08 \pm 0.04$ and $\lambda_4 = -2.8 \pm 0.3$, are similar, being equal to 53.4 $\pm$ 0.1° and 13.8 $\pm$ 0.6°, respectively. The estimate of the orientational distribution relying on the truncated expansion in Legendre polynomials (Figure 7C) assumes negative values for low α, precluding rigorous evaluation of the mean value and standard deviation.

Orientational 1PE TDM Distribution from QM Calculations and MD Simulations. Having determined the 1PE TDM orientation relative to the geometry of the dye molecule, we were able to use our MD trajectories to determine the distribution of the 1PE TDM tilt angle α from the simulations. The results are histogrammed in Figure 7, showing the orientational distribution constructed from all four MD trajectories (the tilt angle distribution for individual trajectories can be found in Supporting Information). The tilt angle distributions constructed from MD trajectories are consistent with a mean tilt angle of 48 $\pm$ 4° and a standard deviation of 13 $\pm$ 2°. Thus, the mean value of α obtained by a combination of QM calculations and MD simulations differs from the value obtained from FDLD measurements by less than 6°, and the standard deviations of the distributions practically coincide (Figure 8). Overall shapes of the tilt angle distributions from simulations and experiments are in a very good agreement with each other, with the Gaussian approximation matching best the simulation results (Figure 7A). The slight discrepancy could be attributed to small inaccuracies in the force field used for

dx.doi.org/10.1021/jp4067026 | J. Phys. Chem. B 2014, 118, 855–863

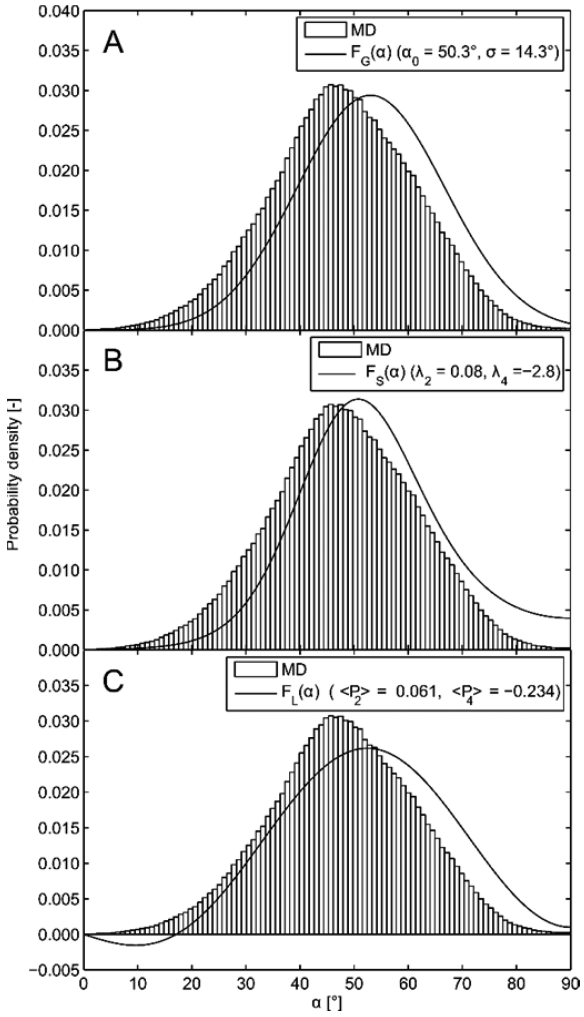

Figure 7. Comparison of the 1PE TDM tilt angle distribution obtained from simulations (histograms) with experimental results based on a (A) Gaussian approximation, (B) entropy-maximizing function, and (C) truncated expansion in Legendre polynomials.

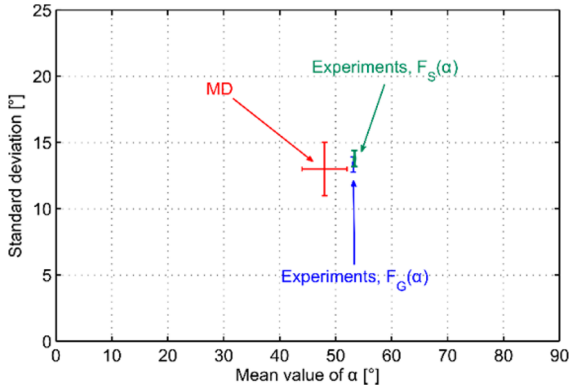

Figure 8. Means and standard deviations of 1PE TDM tilt angle distributions obtained from simulations and experiments ($F_G(\alpha)$ denoting a distribution based on a Gaussian approximation and $F_S(\alpha)$ a distribution based on entropy maximization). The error bars denote 95% confidence intervals.

simulations and experimental factors such as membrane roughness or fluorescence background effects.

CONCLUSIONS

Using 1P and 2P polarization microscopy on F2N12S-labeled GUVs, and a combination of quantum chemistry calculations and molecular dynamics simulations, we have made two independent determinations of the orientational distribution of the one-photon excitation transition dipole moment of this fluorescent dye in a POPC bilayer. Both approaches yield very similar values of the mean 1PE TDM tilt angle with respect to the normal of the membrane, and virtually identical widths of the orientational distributions. The present results thus validate the experimental approach relying on GUVs and FDLD microscopy, and, at least for this particular system, the Gaussian approximation of the 1PE TDM tilt angle distribution. However, an important question remaining to be answered is how generally applicable the commonly assumed Gaussian distribution is. Our results also add credibility to previous determinations of orientational dye distributions made using FDLD microscopy. We conclude that the combination of 1P and 2P polarization microscopy and molecular simulations allows for accurate determination of the orientational 1PE TDM distribution, providing detailed insights into molecular orientations.

Since dye orientation can sensitively report on biophysical properties of its environment (lipid composition, membrane potential, etc.), the present work makes an important contribution toward full exploitation of molecular orientation of a dye as a source of detailed information about the cellular membrane and its biophysical environment. With further work, it should become possible to extend our current studies from fluorescent dyes to fluorescently labeled membrane proteins, and from the simplest model membranes to chemically more complex systems and living cells, ultimately developing FDLD microscopy into a technique capable of yielding detailed quantitative structural information on membrane proteins in living cells.

ASSOCIATED CONTENT

Supporting Information

Further details on computational and experimental procedures and contains additional results of MD trajectory analysis. This material is available free of charge via the Internet at http://pubs.acs.org.

AUTHOR INFORMATION

Corresponding Authors

*E-mail: lazar@nh.cas.cz.

*E-mail: pavel.jungwirth@uochb.cas.cz.

Notes

The authors declare the following competing financial interest(s): Josef Lazar is an owner of Innovative Bioimaging, LLC.

ACKNOWLEDGMENTS

Financial support was provided by the Czech Science Foundation (grant P205/13-10799S to J.L. and grant P208/12/G016 to M.S., M.H., and P.J.) and by the University of South Bohemia (graduate research scholarship 093/2009/P to A.B.). P.J. thanks the Czech Ministry of Education (grant no. LH12001) for support and acknowledges the Academy of Finland for the FiDiPro award. A.B. acknowledges Grant 141/2013/P from the University of South Bohemia. In addition, the

Academy of Sciences is acknowledged for the Praemium Academie award (to P.J. and M.H.).

REFERENCES

(1) Knopfel, T.; Lin, M. Z.; Levskaya, A.; Tian, L.; Lin, J. Y.; Boyden, E. S. Toward the Second Generation of Optogenetic Tools. *J. Neurosci.* **2010**, *30*, 14998−5004.
(2) Cui, L.; Zou, Y.; Lin, N.; Zhu, Z.; Jenkins, G.; Yang, C. J. Mass Amplifying Probe for Sensitive Fluorescence Anisotropy Detection of Small Molecules in Complex Biological Samples. *Anal. Chem.* **2012**, *84*, 5535−5541.
(3) Rusinova, E.; Tretyachenko-Ladokhina, V.; Vele, O. E.; Senear, D. F.; Alexander Ross, J. B. Alexa and Oregon Green Dyes as Fluorescence Anisotropy Probes for Measuring Protein-Protein and Protein-Nucleic Acid Interactions. *Anal. Biochem.* **2002**, *308*, 18−25.
(4) Li, W.; Wang, Y.; Shao, H.; He, Y.; Ma, H. Probing Rotation Dynamics of Biomolecules Using Polarization Based Fluorescence Microscopy. *Microsc. Res. Technol.* **2007**, *70*, 390−395.
(5) Repakova, J.; Capkova, P.; Holopainen, J. M.; Vattulainen, I. Distribution, Orientation, and Dynamics of DPH Probes in DPPC Bilayer. *J. Phys. Chem. B* **2004**, *108*, 13438−13448.
(6) Franova, M.; Repakova, J.; Capkova, P.; Holopainen, J. M.; Vattulainen, I. Effects of DPH on DPPC-Cholesterol Membranes with Varying Concentrations of Cholesterol: From Local Perturbations to Limitations in Fluorescence Anisotropy Experiments. *J. Phys. Chem. B* **2010**, *114*, 2704−2711.
(7) Lazar, J.; Bondar, A.; Timr, S.; Firestein, S. J. Two-Photon Polarization Microscopy Reveals Protein Structure and Function. *Nat. Methods* **2011**, *8*, 684−690.
(8) Steinbach, G.; Pomozi, I.; Zsiros, O.; Pay, A.; Horvath, G. V.; Garab, G. Imaging Fluorescence Detected Linear Dichroism of Plant Cell Walls in Laser Scanning Confocal Microscope. *Cytometry A* **2008**, *73*, 202−208.
(9) DeMay, B. S.; Noda, N.; Gladfelter, A. S.; Oldenbourg, R. Rapid and Quantitative Imaging of Excitation Polarized Fluorescence Reveals Ordered Septin Dynamics in Live Yeast. *Biophys. J.* **2011**, *101*, 985−994.
(10) Benninger, R. K. P.; Onfelt, B.; Neil, M. A. A.; Davis, D. M.; French, P. M. W. Fluorescence Imaging of Two-Photon Linear Dichroism: Cholesterol Depletion Disrupts Molecular Orientation in Cell Membranes. *Biophys. J.* **2005**, *88*, 609−622.
(11) Reeve, J. E.; Corbett, A. D.; Boczarow, I.; Wilson, T.; Bayley, H.; Anderson, H. L. Probing the Orientational Distribution of Dyes in Membranes through Multiphoton Microscopy. *Biophys. J.* **2012**, *103*, 907−917.
(12) Han, Z.; Jin, L.; Turavets, D.; Cohen, L. B.; Lazar, J.; Pieribone, V. A. Modification of Arclight, a Genetically-Encoded Voltage Sensitive Probe: A Study of Mechanism. *Biophys. J.* **2013**, *104*, 679A−680A.
(13) Gasecka, A.; Han, T. J.; Favard, C.; Cho, B. R.; Brasselet, S. Quantitative Imaging of Molecular Order in Lipid Membranes Using Two-Photon Fluorescence Polarimetry. *Biophys. J.* **2009**, *97*, 2854−2862.
(14) Gullapalli, R. R.; Demirel, M. C.; Butler, P. J. Molecular Dynamics Simulations of DiI-C-18(3) in a DPPC Lipid Bilayer. *Phys. Chem. Chem. Phys.* **2008**, *10*, 3548−3560.
(15) Axelrod, D. Carbocyanine Dye Orientation in Red-Cell Membrane Studied by Microscopic Fluorescence Polarization. *Biophys. J.* **1979**, *26*, 557−573.
(16) Klymchenko, A. S.; Duportail, G.; Demchenko, A. P.; Mely, Y. Bimodal Distribution and Fluorescence Response of Environment-Sensitive Probes in Lipid Bilayers. *Biophys. J.* **2004**, *86*, 2929−2941.
(17) Klymchenko, A. S.; Mely, Y.; Demchenko, A. P.; Duportail, G. Simultaneous Probing of Hydration and Polarity of Lipid Bilayers with 3-Hydroxyflavone Fluorescent Dyes. *Biochim. Biophys. Acta, Biomembr.* **2004**, *1665*, 6−19.
(18) Chou, P. T.; Pu, S. C.; Cheng, Y. M.; Yu, W. S.; Yu, Y. C.; Hung, F. T.; Hu, W. P. Femtosecond Dynamics on Excited-State Proton Charge-Transfer Reaction in 4′-N,N-Diethylamino-3-Hydroxyflavone. The Role of Dipolar Vectors in Constructing a Rational Mechanism. *J. Phys. Chem. A* **2005**, *109*, 3777−3787.
(19) Das, R.; Klymchenko, A. S.; Duportail, G.; Mely, Y. Excited state proton transfer and solvent relaxation of a 3-hydroxyflavone probe in lipid bilayers. *J. Phys. Chem. B* **2008**, *112* (38), 11929−11935.
(20) Shynkar, V. V.; Klymchenko, A. S.; Kunzelmann, C.; Duportail, G.; Muller, C. D.; Demchenko, A. P.; Freyssinet, J. M.; Mely, Y. Fluorescent Biomembrane Probe for Ratiometric Detection of Apoptosis. *J. Am. Chem. Soc.* **2007**, *129*, 2187−2193.
(21) Klymchenko, A. S.; Oncul, S.; Didier, P.; Schaub, E.; Bagatolli, L.; Duportail, G.; Mely, Y. Visualization of Lipid Domains in Giant Unilamellar Vesicles Using an Environment-Sensitive Membrane Probe Based on 3-Hydroxyflavone. *Biochim. Biophys. Acta, Biomembr.* **2009**, *1788*, 495−499.
(22) Oncul, S.; Klymchenko, A. S.; Kucherak, O. A.; Demchenko, A. P.; Martin, S.; Dontenwill, M.; Arntz, Y.; Didier, P.; Duportail, G.; Mely, Y. Liquid Ordered Phase in Cell Membranes Evidenced by a Hydration-Sensitive Probe: Effects of Cholesterol Depletion and Apoptosis. *Biochim. Biophys. Acta, Biomembr.* **2010**, *1798*, 1436−1443.
(23) Corry, B.; Jayatilaka, D.; Martinac, B.; Rigby, P. Determination of the Orientational Distribution and Orientation Factor for Transfer Between Membrane-Bound Fluorophores Using a Confocal Microscope. *Biophys. J.* **2006**, *91*, 1032−1045.
(24) Lakowicz, J. R. *Principles of Fluorescence Spectroscopy*, 3rd ed.; Springer: New York, 2006.
(25) Drobizhev, M.; Meng, F. Q.; Rebane, A.; Stepanenko, Y.; Nickel, E.; Spangler, C. W. Strong Two-Photon Absorption in New Asymmetrically Substituted Porphyrins: Interference Between Charge-Transfer and Intermediate-Resonance Pathways. *J. Phys. Chem. B* **2006**, *110*, 9802−9814.
(26) Drobizhev, M.; Makarov, N. S.; Tillo, S. E.; Hughes, T. E.; Rebane, A. Two-Photon Absorption Properties of Fluorescent Proteins. *Nat. Methods* **2011**, *8*, 393−399.
(27) Rebane, A.; Makarov, N. S.; Drobizhev, M.; Spangler, B.; Tarter, E. S.; Reeves, B. D.; Spangler, C. W.; Meng, F. Q.; Suo, Z. Y. Quantitative Prediction of Two-Photon Absorption Cross Section Based on Linear Spectroscopic Properties. *J. Phys. Chem. C* **2008**, *112*, 7997−8004.
(28) Castanho, M.; Lopes, S.; Fernandes, M. Using UV-Vis. Linear Dichroism to Study the Orientation of Molecular Probes and Biomolecules in Lipidic Membranes. *Spectroscopy* **2003**, *17*, 377−398.
(29) Van der Meer, W.; Pottel, H.; Herreman, W.; Ameloot, M.; Hendrickx, H.; Schroder, H. Effect of Orientational Order on the Decay of the Fluorescence Anisotropy in Membrane Suspensions: A New Approximate Solution of the Rotational diffusion Equation. *Biophys. J.* **1984**, *46*, 515−523.
(30) Hess, B.; Kutzner, C.; van der Spoel, D.; Lindahl, E. GROMACS 4: Algorithms for Highly Efficient, Load-Balanced, and Scalable Molecular Simulation. *J. Chem. Theory Comput.* **2008**, *4*, 435−447.
(31) Hoover, W. G. Canonical Dynamics - Equilibrium Phase-Space Distributions. *Phys. Rev. A* **1985**, *31*, 1695−167.
(32) Parrinello, M.; Rahman, A. Polymorphic Transitions in Single-Crystals - a New Molecular-Dynamics Method. *J. Appl. Phys.* **1981**, *52*, 7182−7190.
(33) Hess, B.; Bekker, H.; Berendsen, H. J. C.; Fraaije, J. LINCS: A linear Constraint Solver for Molecular Simulations. *J. Comput. Chem.* **1997**, *18*, 1463−1472.
(34) Miyamoto, S.; Kollman, P. A. Settle - an Analytical Version of the Shake and Rattle Algorithm for Rigid Water Models. *J. Comput. Chem.* **1992**, *13*, 952−962.
(35) Darden, T.; York, D.; Pedersen, L. Particle Mesh Ewald - an N.Log(N) Method for Ewald Sums in Large Systems. *J. Chem. Phys.* **1993**, *98*, 10089−10092.
(36) Becke, A. D. Density-Functional Thermochemistry. III. The Role of Exact Exchange. *J. Chem. Phys.* **1993**, *98*, 5648−5652.
(37) Dunning, T. H. Gaussian Basis Sets for Use in Correlated Molecular Calculations. I. The Atoms Boron through Neon and Hydrogen. *J. Chem. Phys.* **1989**, *90*, 1007−1023.

(38) Frisch, M. J.; Trucks, G. W.; Schlegel, H. B.; Scuseria, G. E.; Robb, M. A.; Cheeseman, J. R.; Scalmani, G.; Barone, V.; Mennucci, B.; Petersson, G. A.et al. *Gaussian 09*, Revision A.02; Gaussian, Inc.: Wallingford CT, 2009.
(39) Singh, U. C.; Kollman, P. A. An Approach to Computing Electrostatic Charges for Molecules. *J. Comput. Chem.* **1984**, *5*, 129−145.
(40) Schuttelkopf, A. W.; van Aalten, D. M. F. PRODRG: A Tool for High-Throughput Crystallography of Protein-Ligand Complexes. *Acta Crystallogr., Sect. D* **2004**, *60*, 1355−1363.
(41) van Gunsteren, W. F.; Berendsen, H. J. C., Gromos-87 manual; Biomos BV: Groningen, The Netherlands, 1987.
(42) van Buuren, A. R.; Marrink, S. J.; Berendsen, H. J. C. A Molecular Dynamics Study of the Decane/Water Interface. *J. Phys. Chem.* **1993**, *97*, 9206−9212.
(43) Mark, A. E.; van Helden, S. P.; Smith, P. E.; Janssen, L. H. M.; van Gunsteren, W. F. Convergence Properties of Free Energy Calculations: Alpha-Cyclodextrin Complexes as a Case Study. *J. Am. Chem. Soc.* **1994**, *116*, 6293−6302.
(44) Berger, O.; Edholm, O.; Jahnig, F. Molecular Dynamics Simulations of a Fluid Bilayer of Dipalmitoylphosphatidylcholine at Full Hydration, Constant Pressure, and Constant Temperature. *Biophys. J.* **1997**, *72*, 2002−2013.
(45) Berendsen, H. J. C.; Postma, J. P. M.; van Gunsteren, W. F.; Hermans, J. Interaction models for water in relation to protein hydration. In *Intermolecular Forces*, Pullman, B., Ed.; D. Reidel Publishing Company: Dordrecht, 1981; pp 331−42.
(46) Casida, M. E., Time-Dependent Density-Functional Response Theory for Molecules. In *Recent Advances in Density Functional Methods (Part I)*, Chong, D. P., Ed.; World Scientific: Singapore, 1995; p 155.
(47) Bauernschmitt, R.; Ahlrichs, R. Treatment of Electronic Excitations Within the Adiabatic Approximation of Time Dependent Density Functional Theory. *Chem. Phys. Lett.* **1996**, *256*, 454−464.
(48) Furche, F.; Ahlrichs, R. Adiabatic Time-Dependent Density Functional Methods for Excited State Properties. *J. Chem. Phys.* **2002**, *117*, 7433−7447.
(49) Runge, E.; Gross, E. K. U. Density-Functional Theory for Time-Dependent Systems. *Phys. Rev. Lett.* **1984**, *52*, 997−1000.
(50) Schafer, A.; Horn, H.; Ahlrichs, R. Fully Optimized Contracted Gaussian-Basis Sets for Atoms Li to Kr. *J. Chem. Phys.* **1992**, *97*, 2571−2577.
(51) Cwiklik, L.; Aquino, A. J. A.; Vazdar, M.; Jurkiewicz, P.; Pittner, J.; Hof, M.; Lischka, H. Absorption and Fluorescence of PRODAN in Phospholipid Bilayers: A Combined Quantum Mechanics and Classical Molecular Dynamics Study. *J. Phys. Chem. A* **2011**, *115*, 11428−11437.
(52) O'Boyle, N. M.; Banck, M.; James, C. A.; Morley, C.; Vandermeersch, T.; Hutchison, G. R. Open Babel: An open chemical toolbox. *J. Chem. Inf.* **2011**, *3*, 33−46.
(53) Angelova, M. I.; Dimitrov, D. S. Liposome Electroformation. *Faraday Discuss.* **1986**, *81*, 303−311.
(54) Stockl, M.; Nikolaus, J.; Herrmann, A. Visualization of Lipid Domain-Specific Protein Sorting in Giant Unilamellar Vesicles. *Liposomes: Methods and Protocols, Vol 2: Biological Membrane Models* **2010**, *606*, 115−126.
(55) Delgado-Gonzalo, R.; Thevenaz, P.; Seelamantula, C. S.; Unser, M. Snakes With an Ellipse-Reproducing Property. *IEEE Transactions on Image Processing* **2012**, *21*, 1258−1271.
(56) Delgado-Gonzalo, R.; Thevenaz, P.; Unser, M. Exponential Splines and Minimal-Support Bases for Curve Representation. *Computer Aided Geometric Design* **2012**, *29*, 109−128.
(57) de Chaumont, F.; Dallongeville, S.; Chenouard, N.; Herve, N.; Pop, S.; Provoost, T.; Meas-Yedid, V.; Pankajakshan, P.; Lecomte, T.; Le Montagner, Y.; et al. Icy: An Open Bioimage Informatics Platform for Extended Reproducible Research. *Nat. Methods* **2012**, *9*, 690−696.
(58) Kulakowska, A.; Jurkiewicz, P.; Sykora, J.; Benda, A.; Mely, Y.; Hof, M. Fluorescence Lifetime Tuning-A Novel Approach to Study Flip-Flop Kinetics in Supported Phospholipid Bilayers. *J. Fluoresc.* **2010**, *20*, 563−569.